Neuron

Article

Orchestrating Opiate-Associated Memories in Thalamic Circuits

Graphical Abstract

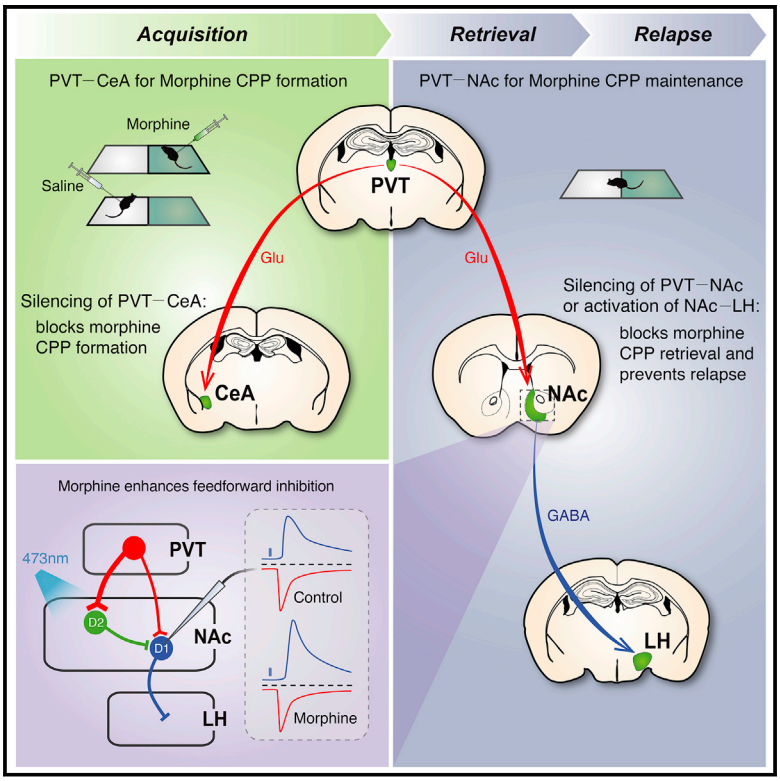

Highlights

- The PVT→CeA pathway associates opiate reward to the environment
- Manipulation of the PVT→NAc or NAc→LH pathway prevents opiate-primed relapse
- Repeated opiate use enhances feedforward inhibition from PVT to the NAc→LH pathway
- iDISCO$^+$ mapping reveals brain-wide networks for storing opiate-associated memories

Authors

Piper C. Keyes, Eliza L. Adams, Zijun Chen, ..., Marc Tessier-Lavigne, Yingjie Zhu, Xiaoke Chen

Correspondence

yj.zhu1@siat.ac.cn (Y.Z.), xkchen@stanford.edu (X.C.)

In Brief

Keyes et al. establish the PVT as a key node in the opiate-associated memory network. The PVT→CeA pathway associates opiate reward to the environment, whereas transient manipulation of the PVT→NAc pathway or its downstream NAc→LH pathway during retrieval erases opiate-associated memory and causes enduring protection against relapse to opioid use.

Keyes et al., 2020, Neuron *107*, 1–11
September 23, 2020
https://doi.org/10.1016/j.neuron.2020.06.028

CellPress

Please cite this article in press as: Keyes et al., Orchestrating Opiate-Associated Memories in Thalamic Circuits, Neuron (2020), https://doi.org/10.1016/j.neuron.2020.06.028

Neuron

CellPress

Article

Orchestrating Opiate-Associated Memories in Thalamic Circuits

Piper C. Keyes,[1] Eliza L. Adams,[1] Zijun Chen,[2] Linlin Bi,[3] Gregory Nachtrab,[3] Vickie J. Wang,[3] Marc Tessier-Lavigne,[3] Yingjie Zhu,[2,3,*] and Xiaoke Chen[1,3,4,*]

[1]Neurosciences Graduate Program, Stanford University, Stanford, CA 94305, USA

[2]Shenzhen Key Laboratory of Drug Addiction, CAS Key Laboratory of Brain Connectome and Manipulation, the Brain Cognition and Brain Disease Institute (BCBDI), Shenzhen Institutes of Advanced Technology, Chinese Academy of Sciences; Shenzhen-Hong Kong Institute of Brain Science-Shenzhen Fundamental Research Institutions, Shenzhen 518055, China

[3]Department of Biology, Stanford University, Stanford, CA 94305, USA

[4]Lead Contact

*Correspondence: yj.zhu1@siat.ac.cn (Y.Z.), xkchen@stanford.edu (X.C.)

https://doi.org/10.1016/j.neuron.2020.06.028

SUMMARY

Disrupting memories that associate environmental cues with drug experiences holds promise for treating addiction, yet accessing the distributed neural network that stores such memories is challenging. Here, we show that the paraventricular nucleus of the thalamus (PVT) orchestrates the acquisition and maintenance of opiate-associated memories via projections to the central nucleus of the amygdala (CeA) and nucleus accumbens (NAc). PVT→CeA activity associates morphine reward to the environment, whereas transient inhibition of the PVT→NAc pathway during retrieval causes enduring protection against opiate-primed relapse. Using brain-wide activity mapping, we revealed distributed network activities that are altered in non-relapsing mice, which enabled us to find that activating the downstream NAc→lateral hypothalamus (LH) pathway also prevents relapse. These findings establish the PVT as a key node in the opiate-associated memory network and demonstrate the potential of targeting the PVT→NAc→LH pathway for treating opioid addiction.

INTRODUCTION

A major challenge for treating addiction is to prevent relapse, which occurs largely due to the retrieval of powerful memories that associate drug-evoked experiences with their proximal environmental cues (Milton and Everitt, 2012; White, 1996). Drug-associated memories are formed and recalled by distributed neural networks (Koob and Volkow, 2010; Lüscher, 2016), but how their activity is coordinated remains uncertain. To orchestrate these networks, a region of the brain must be extensively connected with both cognitive and visceral areas as well as project to multiple nuclei involved in drug-associated behaviors or memories. The paraventricular nucleus of the thalamus (PVT) integrates top-down information from prefrontal and insular cortices and bottom-up information from hypothalamic and brainstem regions that convey motivational arousal and homeostatic states (Kirouac, 2015; Li and Kirouac, 2008). In turn, the PVT innervates all structures in the extended amygdala system, including the central nucleus of the amygdala (CeA) and nucleus accumbens (NAc) (Kirouac, 2015; Li and Kirouac, 2008), whose roles in drug addiction have been extensively studied (Kirouac, 2015; Koob and Volkow, 2010; Lüscher, 2016). While it has been suggested that the PVT contributes to drug-seeking behavior (Kirouac, 2015; Millan et al., 2017), the roles of each PVT pathway at different stages of drug-associated memories have not been systematically investigated.

Opioid abuse in the United States has reached epidemic levels and become a major public health issue (Rudd et al., 2016). When taking an opioid, the immediate rewarding effects are followed by the emergence of an acute withdrawal state as the drug is metabolized. The positive reinforcement of opioid reward as well as the negative reinforcement of avoiding withdrawal could promote the formation and maintenance of drug-associated memories (Evans and Cahill, 2016; Wise and Koob, 2014). Although the role of reward in drug seeking is well established, the contribution of drug withdrawal remains debatable. It has been hypothesized that opioid users learn to associate opioid intake with relief from negative withdrawal states, and this maladaptive association could last long after acute withdrawal symptoms have terminated and underlie the drug cravings experience by many users after exposure to drug-associated cues or stressful life events (Evans and Cahill, 2016). We recently identified the PVT→NAc pathway as a critical mediator of opiate withdrawal (Zhu et al., 2016), which affords a unique opportunity to directly test this long-standing hypothesis. In addition to the NAc pathway, the PVT could influence drug-associative

Please cite this article in press as: Keyes et al., Orchestrating Opiate-Associated Memories in Thalamic Circuits, Neuron (2020), https://doi.org/10.1016/j.neuron.2020.06.028

memories through its connection to the CeA. The CeA is important for associating cues with both appetitive and aversive outcomes (Fadok et al., 2018), and the PVT→CeA pathway is required for fear conditioning (Do-Monte et al., 2015; Penzo et al., 2015). However, whether the same pathway is also required for opiate-associated memory is unknown.

In the present study, we combined morphine conditioned place preference (CPP) training and pathway-specific manipulation to delineate roles of each PVT output pathway in the formation and maintenance of morphine CPP. We found that activity in the PVT→CeA pathway does not drive reward but is required for associating opiate use to the environment, whereas the PVT→NAc pathway is essential for the retrieval and maintenance of morphine CPP. Transient inhibition of this pathway during retrieval has a lasting protective effect against morphine-primed relapse, suggesting a potent circuitry target for treating opioid addiction. Moreover, whole-brain c-Fos mapping revealed a distributed neural network that is activated by morphine relapse, including the lateral hypothalamus (LH). Repeated morphine exposure converted PVT input from excitation to inhibition of the NAc→LH pathway, and optogenetic activation of this pathway also blocked memory retrieval and prevented relapse. Our results demonstrate functional dissociation of distinct PVT output pathways in controlling the formation and maintenance of opiate-associated memory and establish the PVT→NAc→LH pathway as a potent target for preventing relapse to opiate use.

RESULTS

The PVT→CeA Pathway Is Required for CPP Formation

We employed a standard and robust morphine CPP protocol (Tzschentke, 2007), which consisted of training mice with four daily intraperitoneal (i.p.) injections of saline and 45 min of confinement to one side of a CPP training chamber in the morning, followed by an injection of morphine (15 mg/kg, i.p.) and 45 min of confinement to the other side of the chamber at least 4 h later (Figures 1A, 2A, 3A, and 5E). To assess activity of PVT output pathways, we transduced PVT neurons with an adeno-associated virus (AAV) expressing a genetic encoded Ca^{2+} indicator (AAV-GCaMP6m) (Chen et al., 2013) and implanted optical fibers onto the terminals areas in the CeA and NAc. Using fiber photometry (Cui et al., 2013; Gunaydin et al., 2014), we recorded population Ca^{2+} signals from the PVT→CeA and PVT→NAc pathways for 20 min during training and retrieval of morphine CPP and found robust calcium signals in both pathways (Figures S1A and S1B).

Because PVT output pathways were activated during CPP training and retrieval, we therefore employed chemogenetic and optogenetic pathway inhibition to examine the contribution of different PVT outputs to each stage of morphine-associated memories. To inhibit PVT output pathways, we injected AAV encoding a chemogenetic inhibitory DREADD (designer receptor exclusively activated by designer drugs; AAV-hM4D) into the PVT (Armbruster et al., 2007; Stachniak et al., 2014) and cannulated onto the terminals areas in the CeA and NAc (Figures 1B, 2B, and S2A–S2F). We performed whole-cell recording in acute CeA slices containing hM4D-expressing terminals from the PVT to validate the efficacy of chemogenetic terminal inhibition. We found that perfusion of the synthetic hM4D ligand, clozapine-N-oxide (CNO; 3 μM) significantly suppressed the excitatory postsynaptic currents (EPSCs) in CeA neurons (Figure S3A) (Zhu et al., 2016), indicating that CNO has effectively inhibited neurotransmission from the hM4D-expressing terminals.

We first investigated the role of the PVT→CeA pathway in the formation of opiate-associated memory (Figures 1A and 1B). 20 min before each morphine pairing trial, we infused CNO (3 μM, 200 nL) locally through the cannula to inhibit the PVT→CeA pathway during training. With local infusion of CNO into the CeA during each morphine CPP training session, we observed a significant reduction of the CPP score tested the day after last training session in hM4D-expressing, but not RFP-expressing, mice (Figure 1C). We then investigated role of the PVT→CeA pathway in morphine CPP retrieval. Different group of mice injected with AAV-hM4D in the PVT were first trained with robust morphine CPP (Figure 1D, test 1). 1 day later, we infused CNO or saline through the cannula to the CeA 20 min before the retrieval test (test 2) and found no difference in CPP retrieval between CNO- or saline-infused mice (Figure 1D, test 2). On the following day, in the absence of inhibition, there was also no difference between the two groups (Figure 1D, test 3). These results demonstrate that activity in the PVT→CeA pathway contributes selectively to the formation of morphine CPP.

The PVT→CeA Pathway Drives Association

The failure to form a robust morphine CPP may be due either to a decrease in the reward value of morphine or an impairment of associating morphine reward with its paired chamber. Inhibition of the PVT→CeA pathway had no effect on the psychostimulant effect of morphine or the reward value of palatable food, as measured by morphine-induced locomotor activity (Figure 1E) and consumption of palatable food in satiated mice (Figure 1F), respectively. We test the second scenario by optogenetically activating the PVT→CeA pathway during a suboptimal CPP paradigm, which consisted of a lower morphine dose (5 mg/kg, i.p.) and shorter confinement time (15 min) for three training days. Optogenetic stimulation of channelrhodopsin2 (ChR2) (Boyden et al., 2005) expressing terminals from the PVT-evoked robust CNQX (6-Cyano-7-nitroquinoxaline-2,3-dione) -sensitive EPSCs in CeA neurons (Figures S3B and S3C), but optogenetic stimulation of the PVT→CeA pathway in freely moving mice had no effect on the time spent in the light-stimulated chamber (Figure S3D), suggesting that the activation of the PVT→CeA pathway is not reinforcing. Interestingly, light stimulation of the same pathway during each morphine pairing of the suboptimal CPP significantly increased the CPP score in ChR2-expressing, but not EGFP-expressing, mice (Figure 1G). Optogenetic stimulation had no effect on locomotor activity (Figure 1H). Together, these results indicate that the PVT→CeA pathway associates the incentive salience of morphine to its paired environment.

Inhibition of the PVT→NAc Pathway Prevents Relapse

Using a similar CPP protocol and chemogenetic pathway inhibition as described above, we next examined the role of the PVT→NAc pathway in the formation and retrieval of

Please cite this article in press as: Keyes et al., Orchestrating Opiate-Associated Memories in Thalamic Circuits, Neuron (2020), https://doi.org/10.1016/j.neuron.2020.06.028

CellPress

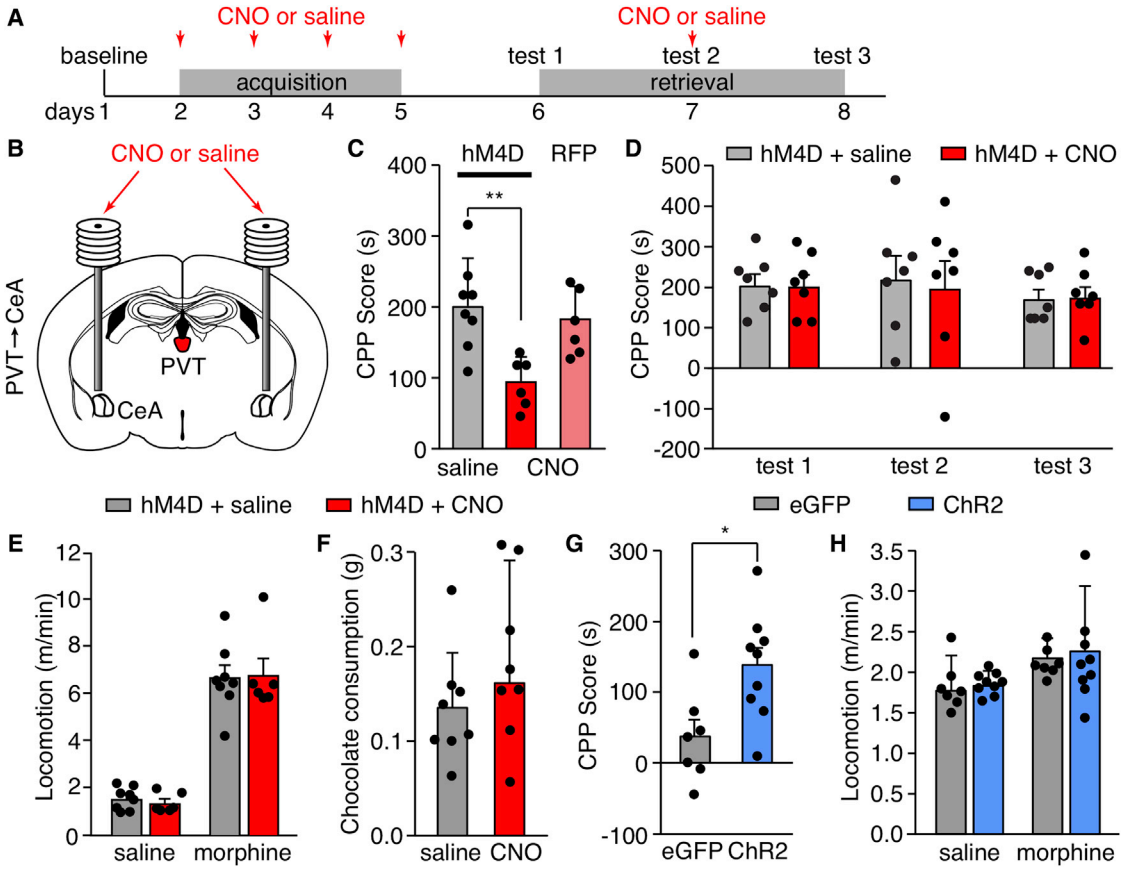

Figure 1. The PVT→CeA Pathway Mediates Morphine Reward Memory Formation

(A) Experimental timeline for (C) and (D). Red arrows mark local infusion of CNO or saline into the CeA during each morphine paring trial (C) or during retrieval test 2 (D).

(B) Schematics of *in vivo* chemogenetic inhibition of the PVT→CeA pathway.

(C) CPP score was reduced by local infusion of CNO into the CeA of hM4D-expressing mice (red, n = 8), but not td-Tomato-expressing mice (light red, n = 6), or local infusion of saline (black, n = 6) into hM4D-expressing mice. One-way ANOVA ($F_{(2,19)} = 4.632$, p = 0.0034) followed by Dunnett's multiple comparisons test. **p < 0.01.

(D) Local infusion of CNO (red, n = 7) or saline (black, n = 7) into the CeA of hM4D-expressing mice during test 2 had no effect on CPP scores on tests 2 and 3. Two-way ANOVA (main effect of group $F_{(1,12)} = 0.0351$, p = 0.8545; main effect of test $F_{(2,24)} = 0.6666$, p = 0.5227; interaction $F_{(2,24)} = 0.0792$, p = 0.9241) with post hoc multiple comparisons with Bonferroni corrections.

(E) Local infusion of saline (black, n = 8) or CNO (red, n = 6) into the CeA of hM4D-expressing mice had no effect on morphine-induced increase of locomotion; multiple t test.

(F) Local infusion of saline (black, n = 8) or CNO (red, n = 8) into the CeA of hM4D-expressing mice had no effect on chocolate consumption; paired t test, two tailed.

(G) Light stimulation of the PVT→CeA pathway during suboptimal morphine CPP training significantly increased the CPP score in ChR2-expressing mice (blue, n = 9), but not EGFP-expressing mice (black, n = 7) (unpaired t test, two-tailed [p = 0.0235]). *p < 0.05.

(H) Light stimulation of ChR2- (blue, n = 9) and EGFP-expressing (black, n = 7) mice had no effect on locomotion during subthreshold morphine CPP training; multiple t test.

Data are presented as mean ± SEM.

See also Figures S1–S3 and Table S2.

opiate-associated memories (Figures 2A, 2B, and S2G). In contrast to inhibition of the PVT→CeA pathway (Figure 1C), local infusion of CNO into the NAc of hM4D-expressing mice during each morphine training had no effect on the CPP score when compared to saline-infusion controls (Figure 2C). However, in mice that expressed a robust morphine CPP after training (Figure 2D, day 6, test 1), chemogenetic inhibition of the PVT→NAc pathway during test 2 impaired retrieval of opiate-associated memories (Figure 2D, day 7, test 2), again in contrast to inhibition of the PVT→CeA pathway (Figure 1D). Surprisingly, when these mice were tested again on day 8 without chemogenetic inhibition, their preference for morphine-paired chamber was still lost (Figure 2D, test 3), suggesting that transient pathway inhibition disrupted the maintenance of morphine memory. We sought to examine how robust this memory impairment would be to other cues. Compared to environmental cues,

Please cite this article in press as: Keyes et al., Orchestrating Opiate-Associated Memories in Thalamic Circuits, Neuron (2020), https://doi.org/10.1016/j.neuron.2020.06.028

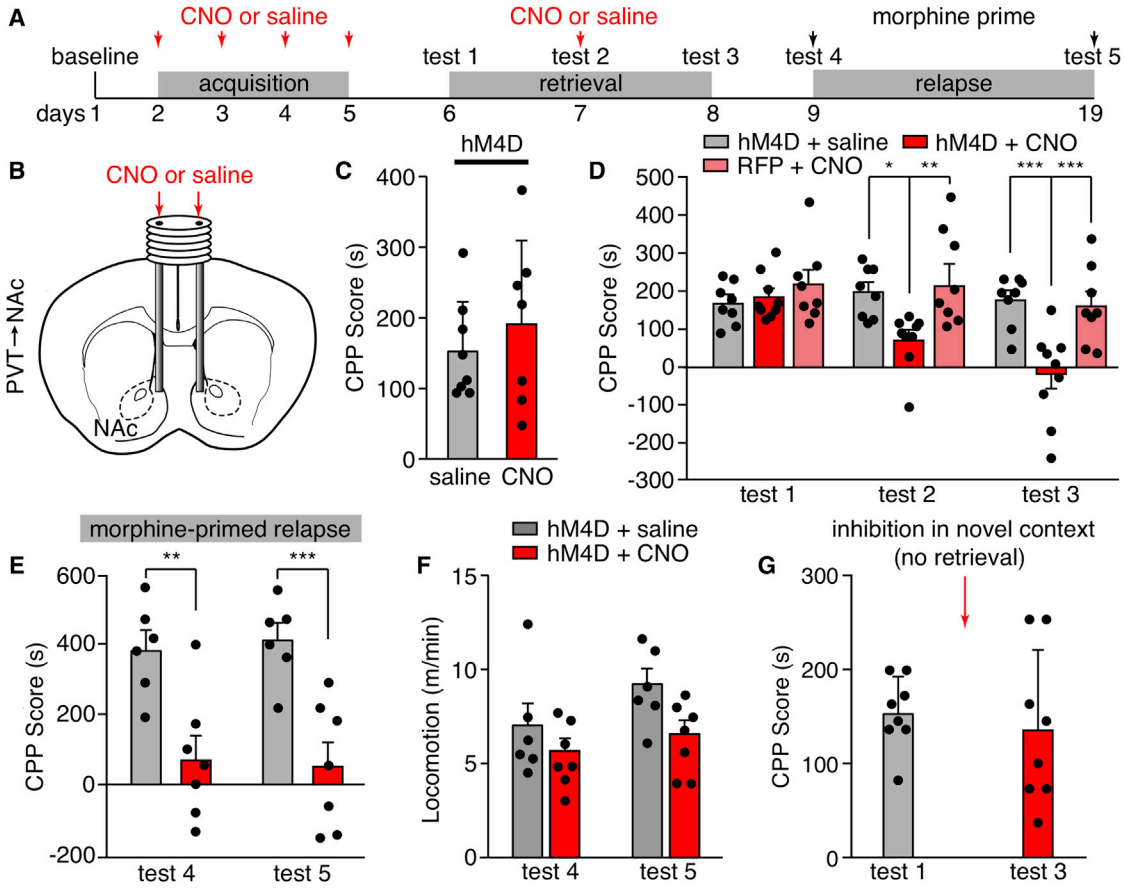

Figure 2. hM4D-Mediated PVT→NAc Pathway Inhibition Prevents Retrieval and Relapse

(A) Experimental timeline for (C)–(E). Red arrows mark local infusion of CNO or saline into the NAc during each morphine paring trial (C) or during the retrieval test 2 (D). Black arrows mark morphine prime injection.

(B) Schematics of *in vivo* chemogenetic inhibition of the PVT→NAc pathway.

(C) Local infusion of saline (black, n = 8) and CNO (red, n = 7) into the NAc of hM4D-expressing mice had no effect on CPP scores; unpaired two-tailed t test.

(D) CPP score was reduced by local infusion of CNO into the NAc during test 2 of hM4D-expressing mice (red, n = 9), but not td-Tomato-expressing mice (light red, n = 8), or local infusion of saline (black, n = 8) into hM4D-expressing mice. Two-way ANOVA (main effect of group $F_{(2,22)} = 8.124$, p = 0.0023; main effect of test $F_{(2,44)} = 7.005$, p = 0.0023; interaction $F_{(2,44)} = 4.03$, p = 0.0072) with post hoc multiple comparisons with Bonferroni corrections. *p < 0.05; **p < 0.01; ***p < 0.001.

(E) Morphine-priming injection (10 mg/kg) induces robust relapse of CPP in saline-infused (black, n = 6), but not CNO-infused (red, n = 7), hM4D-expressing mice. Two-way ANOVA (main effect of group $F_{(1,11)} = 18.85$, p = 0.0012; main effect of test $F_{(1,11)} = 0.0169$, p = 0.8989; interaction $F_{(1,11)} = 0.3311$, p = 0.5766) with post hoc multiple comparisons with Bonferroni corrections. **p < 0.01; ***p < 0.001.

(F) No difference was found in morphine-primed increased locomotion between saline- (black, n = 6) and CNO-infused (red, n = 7) mice used in (E); multiple t test.

(G) No difference was found in CPP scores of mice before (black) and after (red) inhibition of the PVT→NAc pathway in a novel context (n = 8; paired t test).

Data are presented as mean ± SEM. See also Figures S1 and S2 and Table S2.

exposure to even a small amount of drug itself is more potent in triggering relapse long after cessation of chronic drug use (Bossert et al., 2013; Shaham et al., 2003; Venniro et al., 2016). Importantly, transient inhibition of the PVT→NAc pathway completely prevented morphine-primed (10 mg/kg, i.p.) relapse at 4 or 14 days of abstinence (Figure 2E) but had no effect on morphine-induced increase of locomotion (Figure 2F). Lastly, when the pathway was inhibited in a novel environment, the mice showed a robust CPP when tested 1 day later (Figure 2G), indicating that memory retrieval is required for PVT→NAc pathway inhibition caused disruption of morphine CPP. Together, these results reveal that activity in the PVT→NAc pathway is required for both the retrieval and maintenance of opiate-associated memories and substantiate the PVT→NAc pathway as a potent target for relapse prevention.

According to memory reconsolidation theory, retrieval can put memories into a labile state, in which they become more susceptible to change (Nader et al., 2000). The labile stage of retrieved memories is a time-dependent process (<6 h after retrieval) called reconsolidation, which provides a time window for updating or disruption of previous memories. Extinction training within the reconsolidation window can also erase fear or drug-associated memories (Monfils et al., 2009; Xue et al., 2012). While single trial chemogenetic inhibition of the PVT→NAc pathway

Please cite this article in press as: Keyes et al., Orchestrating Opiate-Associated Memories in Thalamic Circuits, Neuron (2020), https://doi.org/10.1016/j.neuron.2020.06.028

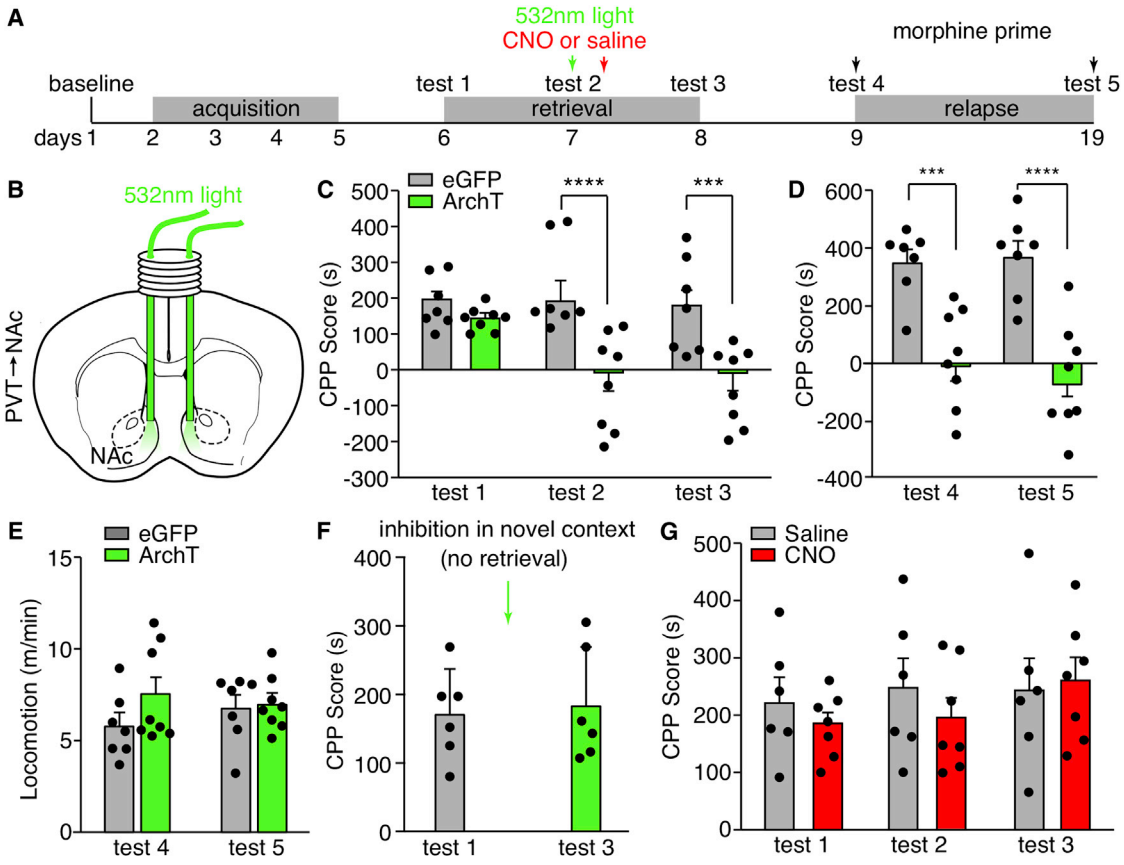

Figure 3. Optogenetic Inhibition of the PVT→NAc Pathway Prevent Retrieval and Relapse

(A) Experimental timeline for (C), (D), and (G). Green arrow marks light stimulation in the NAc during retrieval test 2 (C). Black arrows mark morphine prime injection (D). Red arrow marks local infusion of CNO or saline into the NAc after retrieval test 2 (G).

(B) Schematics of *in vivo* optogenetic inhibition of the PVT→NAc pathway.

(C) Light stimulation during test 2 significantly reduced CPP scores for tests 2 and 3 in ArchT-expressing mice (green, n = 8), but not EGFP-expressing mice (black, n = 7). Two-way ANOVA (main effect of group $F_{(1,45)} = 19.22$, $p < 0.0001$; main effect of test $F_{(2,45)} = 2.645$, $p = 0.0821$; interaction $F_{(2,45)} = 2.312$, $p = 0.1107$) with post hoc multiple comparisons with Bonferroni corrections. ***$p < 0.001$; ****$p < 0.0001$.

(D) Morphine-priming injection (10 mg/kg) induces robust relapse of CPP in EGFP-expressing (black, n = 7), but not ArchT-expressing (green, n = 8), mice. Two-way ANOVA (main effect of group $F_{(1,13)} = 23.13$, $p = 0.0003$; main effect of test $F_{(1,13)} = 1.245$, $p = 0.2847$; interaction $F_{(1,13)} = 3.982$, $p = 0.0674$) with post hoc multiple comparisons with Bonferroni corrections. ***$p < 0.001$; ****$p < 0.0001$.

(E) No difference was found in morphine-primed increased locomotion between EGFP-expressing mice (black, n = 7) and ArchT-expressing mice (green, n = 8) used in (D); multiple t test.

(F) No difference was found in CPP scores of mice before (black) and after (green) inhibiting the PVT→NAc pathway in a novel context. n = 6; paired t test, two-tailed.

(G) No difference was found in CPP scores of mice after local infusion of saline (black, n = 6) or CNO (red, n = 7) into the NAc after test 2 in hM4D-expressing mice. Two-way ANOVA (main effect of group $F_{(1,11)} = 0.2512$, $p = 0.6261$; main effect of test $F_{(2,22)} = 2.016$, $p = 0.1571$; interaction $F_{(2,22)} = 1.267$, $p = 0.3014$) with post hoc multiple comparisons with Bonferroni corrections.

Data are presented as mean ± SEM. See also Figures S1 and S5 and Table S2.

prevented retrieval of opiate-associated memory, hM4D-mediated inhibition is known to have lasting effect (Alexander et al., 2009) and could inhibit the pathway during both the retrieval and reconsolidation windows. We thus sought to inhibit the PVT→NAc pathway selectively during the retrieval or reconsolidation phase. We took advantage of the exquisite time resolution offered by optogenetic tools to transiently inhibit the PVT→NAc pathway during 15-min retrieval. We injected archaerhodopsin-3 (ArchT)- or EGFP-expressing AAV into the PVT and bilaterally implanted fiber guide cannulae in the NAc (Figures 3A, 3B, and S5A) (Chow et al., 2010; Han et al., 2011). 2 weeks after the surgery, the mice were trained to form a robust CPP (Figure 3C, test 1). We then delivered constant light (532 nm, 5 mW mm^{-2}) to the NAc during test 2 and found that morphine CPP was strongly suppressed in ArchT-expressing, but not EGFP-expressing, mice (Figure 3C, test 2). Importantly, transient optogenetic inhibition of the PVT→NAc pathway during test 2 caused memory retrieval blockage (Figure 3C, test 3), and relapse prevention (Figure 3D, tests 4 and 5) was as robust as what was caused by chemogenetic pathway inhibition but had no effect on

Please cite this article in press as: Keyes et al., Orchestrating Opiate-Associated Memories in Thalamic Circuits, Neuron (2020), https://doi.org/10.1016/j.neuron.2020.06.028

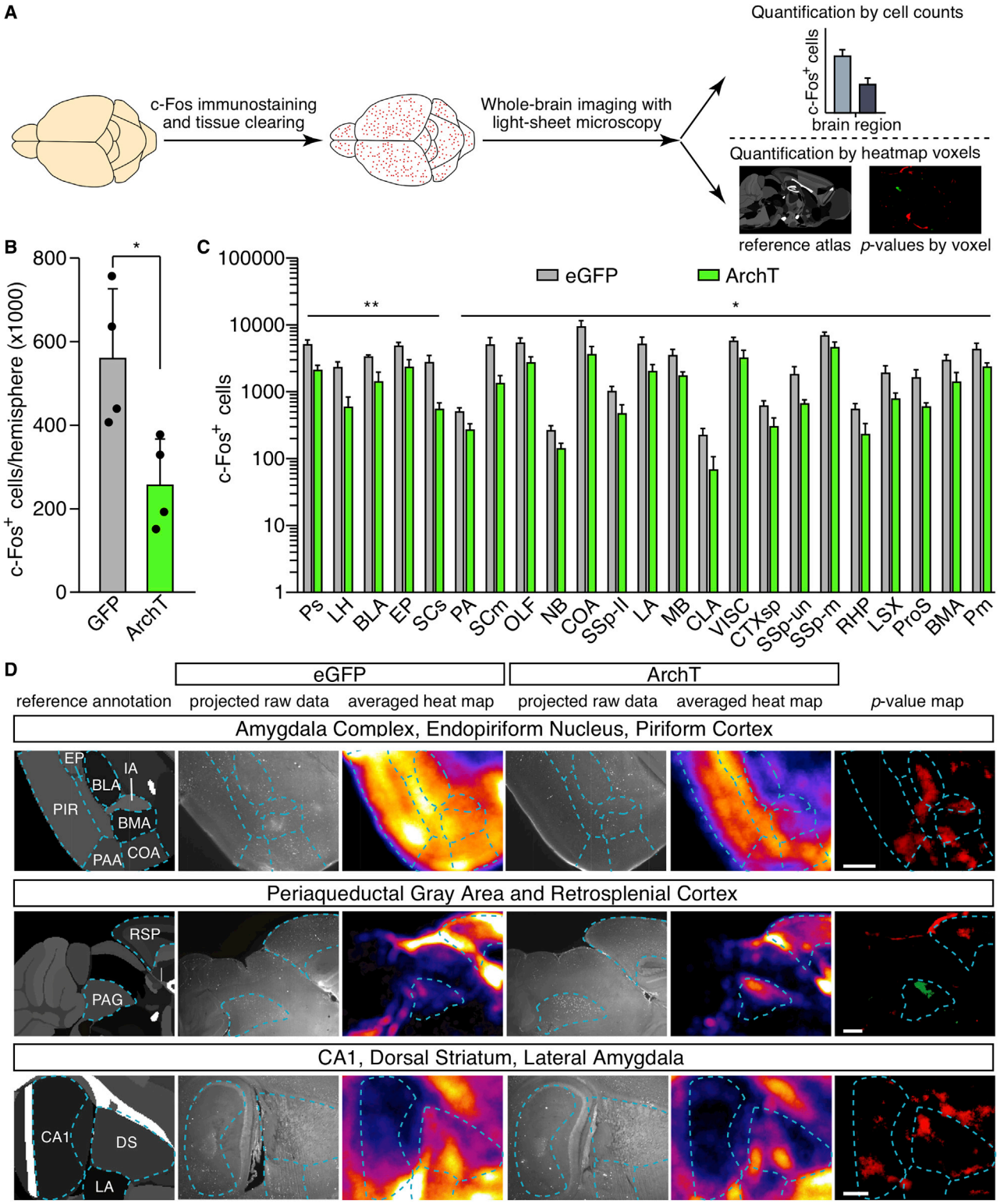

Figure 4. Whole-Brain c-Fos Mapping after Opiate-Primed Relapse

(A) Schematics of iDISCO+ and the ClearMap pipeline.

(B) Quantification shows significantly more total c-Fos+ cells per hemisphere in EGFP-expressing mice (black, n = 4) than ArchT-expressing mice (green, n = 4) after test 5 (unpaired t test [p = 0.0239]). *p < 0.05.

(legend continued on next page)

Please cite this article in press as: Keyes et al., Orchestrating Opiate-Associated Memories in Thalamic Circuits, Neuron (2020), https://doi.org/10.1016/j.neuron.2020.06.028

locomotion (Figure 3E). Again, exposure to the environmental cues was critical, as optogenetic inhibition of the PVT→NAc pathway without memory retrieval had no effect on CPP score tested 24 h later (Figure 3F). We also optogenetically inhibited the PVT→CeA pathway during test 2 and found no effect on CPP retrieval in test 3 (Figures S3E-S3G), which is similar to chemogenetic pathway inhibition (Figure 1D). To inhibit the PVT→NAc pathway during the reconsolidation window, we locally infused CNO into the NAc of hM4D-expressing mice after retrieval (test 2) to inhibit the PVT→NAc pathway during the reconsolidation window but found no effect on CPP score tested 1 day later (Figures 3A and 3G). Additionally, we chemogenetically inhibited the PVT→NAc pathway after the last CPP training and also found no effect on later retrieval tests 1–3 (Figures S1C and S1D). Thus, inhibition of the PVT→NAc pathway during retrieval but not reconsolidation phase is required to block memory retrieval and prevent relapse.

iDISCO$^+$ c-Fos Mapping Opiate-Associated Memory Traces

Drug-associated memories are thought to be stored in distributed brain networks. However, accessing such brain-wide networks is challenging. Inhibition of the PVT→NAc pathway impaired memory retrieval, which should prevent reactivation of its specific memory traces and provide a unique opportunity to access the distributed traces for opiate-associated memories. We thus performed iDISCO$^+$ (immunolabeling-enabled three-dimensional imaging of solvent-cleared organs)-based (Renier et al., 2014, 2016) whole-mount immunolabeling of c-Fos, a marker for recent neuronal activity, to examine the relapse-induced brain-wide activity of mice from the optogenetic inhibition group and the control group (Figure 4A). Mice used in Figure 3D were used for iDISCO$^+$ experiments. 60 min after the last morphine-primed relapse test (test 5, Figure 3D), brains of both groups were harvested and went through the iDISCO$^+$ tissue clearing procedure with immunostaining for c-Fos. The mouse brains were then imaged by a scanning light sheet microscope at a cellular resolution and automatically analyzed with the "ClearMap" program (Renier et al., 2016). Our analysis (brain-region-based cell count and voxel-based p value map; see STAR Methods) revealed that transient PVT→NAc pathway inhibition causes a profound reduction of neurons activated during the relapse test across the whole brain (Figure 4B), including 22 brain regions that showed a significant reduction (Figure 4C; Table S1). This network contains brain regions that have previously been reported to be important for retrieval and reinstatement of drug CPP, such as the amygdala complex and hippocampus, as well as brain regions that have not been associated with morphine-associated memories (Figures 4C and 4D).

Opiate Strengthens Feedforward Inhibition on the NAc→LH Pathway

Among brain regions revealed by c-Fos iDISCO mapping, we were particularly interested in studying the LH, since it is the only NAc downstream structure that showed a significant change in c-Fos expression after transient PVT→NAc pathway inhibition (Figure 5A). Although roles of the NAc→LH pathway in motivated behaviors have recently been characterized (Gibson et al., 2018; O'Connor et al., 2015), its contribution to opioid seeking is still unknown, and how PVT inputs control this pathway has not been studied. Given that chronic morphine selectively strengthens PVT inputs onto D2 medium spiny neurons (MSNs) (Zhu et al., 2016), D2 MSNs provide major lateral inhibition onto neighboring D1-MSN cells (Dobbs et al., 2016), and LH-projecting neurons in the NAc (NAc^{LH} neurons) are largely D1-MSN cells (Figure S4A) (Gibson et al., 2018; O'Connor et al., 2015), we postulated that morphine treatment could increase the feedforward inhibition from the PVT onto the NAc→LH pathway (Figure 5B). To directly test this prediction, we retrogradely labeled the NAc^{LH} neurons by injecting rAAV2-retro-mRuby3 in the LH and injected AAV-ChR2 into the PVT (Tervo et al., 2016). 3 weeks later, these mice were given daily morphine (15 mg/kg) or saline for four consecutive days in their home cage followed by 2 days of abstinence, before we performed slice recording to examine excitability, PVT-evoked EPSCs, inhibitory postsynaptic currents (IPSCs), and the effect of PVT inputs on the action potential (AP) firing of NAc^{LH} neurons. Although morphine had no effect on the excitability of NAc^{LH} neurons (Figures S4B and S4C), we observed a significant increase in the ratio of PVT-evoked IPSCs/EPSCs (Figure 5C) and PVT-evoked miniature IPSCs (mIPSCs) (Figures S4D and S4E) in the NAc^{LH} neurons of morphine- but not saline-treated mice. Moreover, photostimulation of PVT inputs increased AP firing in control mice but suppressed AP firing in morphine-treated mice (Figure 5D). Together, our results show that repeated morphine exposure converts the PVT's drive from excitation to inhibition onto the NAc→LH pathway.

Activation of the NAc→LH Pathway Prevents Relapse

If increased feedforward inhibition onto the NAc→LH pathway is required for the maintenance of morphine-associated memories, then activation of this pathway should have a similar effect as inhibition of the PVT→NAc pathway in preventing relapse. We

(C) Quantification of regions of significant difference in c-Fos expression between ArchT-expressing mice (green) and eGFP-expressing mice (black). p values are presented in Table S1. Abbreviations are as follows: Ps, pons, sensory related; LH, lateral hypothalamus; BLA, basolateral amygdala; BMA, basomedial amygdala; EP, endopiriform nucleus; SCs, superior colliculus, sensory related; PA, posterior amygdala; SCm; superior colliculus, motor related; OLF, olfactory areas; NB, nucleus of the brachium of the inferior colliculus; COA, cortical amygdala; SSp-ll, primary somatosensory area, lower limb; LA, lateral amygdala; MB, midbrain; CLA, claustrum; CTXsp, visceral area, cortical subplate; SSp-un, primary somatosensory area, unassigned; SSp-m, primary somatosensory area, mouth; RHP, retrohippocampal region; LSX, lateral septal complex; ProS, prosubiculum; Pm, pons, motor related; PIR, piriform area; IA, intercalated amygdala; PAA, piriform-amygdalar area; PAG, periaqueductal gray; RSP, retrosplenial cortex; CA1, field CA1; DS, dorsal striatum. *$p < 0.05$; **$p < 0.01$, multiple t tests. (D) Voxel-based statistics on c-Fos density heatmaps. Left panels: reference annotation of regions of interest based on Allen Brain Atlas. Second and fourth panels from the left: 30-μm projections of representative raw c-Fos immunostaining data from EGFP- and ArchT-expressing mice. Third and fifth panels from the left: mean c-Fos density heatmaps. Right panels: P value maps. Red and green voxels indicate a significant decrease and increase, respectively, when comparing the ArchT- to the EGFP-expressing mice. Note green voxels in the PAG. Scale bars, 500 μm.
Data are presented as mean ± SEM.

Please cite this article in press as: Keyes et al., Orchestrating Opiate-Associated Memories in Thalamic Circuits, Neuron (2020), https://doi.org/10.1016/j.neuron.2020.06.028

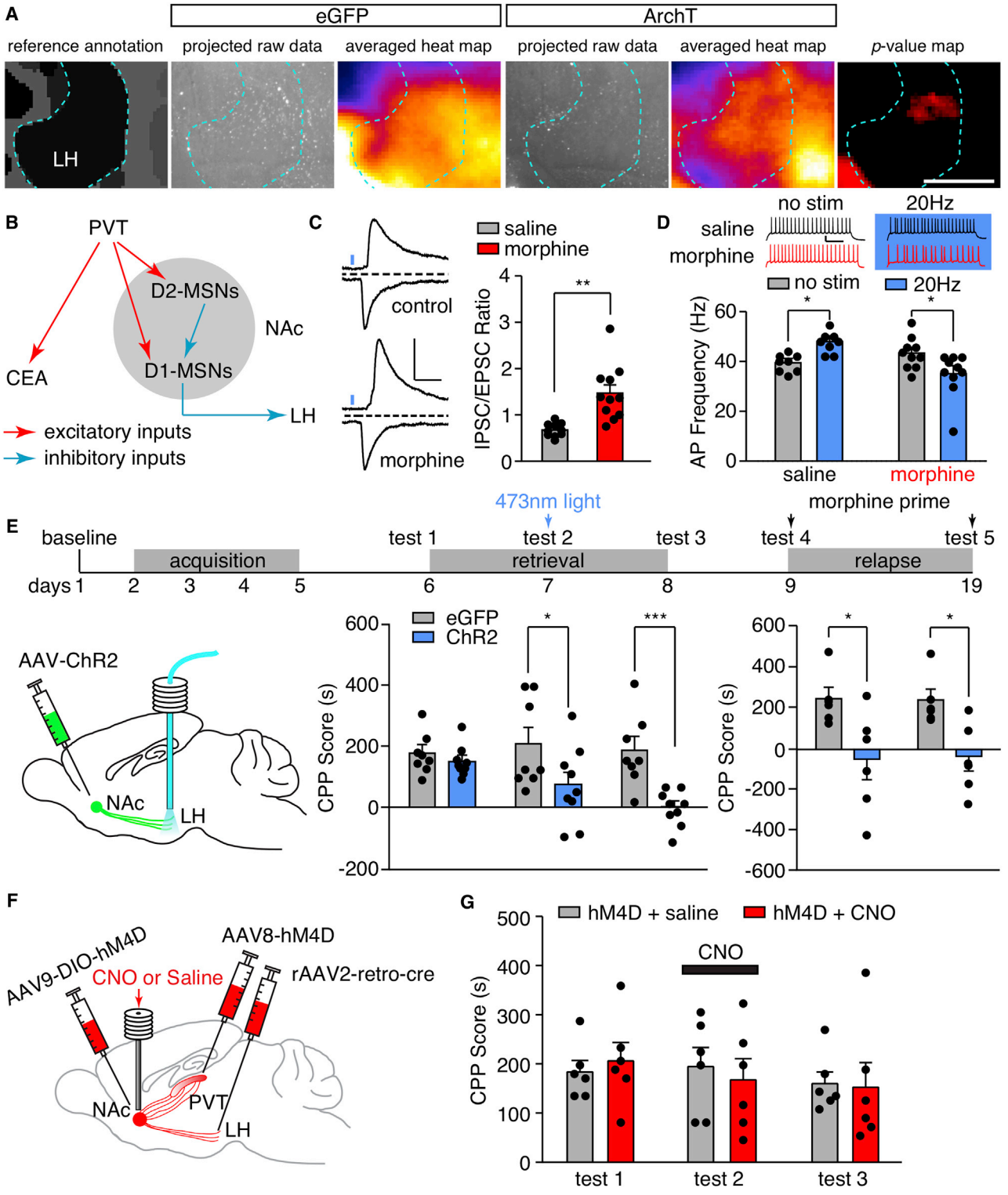

Figure 5. The PVT→NAc→LH Pathway Mediates Morphine Memory Retrieval and Maintenance

(A) Voxel-based statistics on LH. Scale bars, 500 μm.

(B) Schematic of feedforward inhibition from the PVT onto the NAc→LH pathway via D2-MSNs.

(C) Representative traces (left) and quantification (right) shows increase of IPSC/EPSC ratios in NAc^{LH} neurons after morphine (red, n = 11 cells), but not saline (black, n = 10 cells), treatment. Scale bars, 200 pA, 40 ms. **p < 0.01; unpaired t test.

(legend continued on next page)

Please cite this article in press as: Keyes et al., Orchestrating Opiate-Associated Memories in Thalamic Circuits, Neuron (2020), https://doi.org/10.1016/j.neuron.2020.06.028

transduced neurons in the medial shell of the NAc with AAV-ChR2 or AAV-EGFP and cannulated in the LH (Figures S5B–S5E) and then trained these mice to form a robust morphine CPP (test 1, Figure 5E). On day 7, we retested these mice together with bilateral optogenetic stimulation (473 nm, 3 mW, 20 Hz) of the NAc→LH pathway and observed a significant reduction of CPP score in ChR2-expressing, but not EGFP-expressing, mice (test 2, Figure 5E). Moreover, similar to PVT→NAc pathway inhibition, transient activation of the NAc→LH pathway also prevented CPP retrieval when tested 1 day later (test 3, Figure 5E), as well as morphine-primed relapse 4 or 14 days of abstinence (tests 4 and 5, Figure 5E), indicating a long-lasting disruption of morphine-associated memory. Thus, activation of the NAc-LH pathway is sufficient to prevent relapse.

Lastly, we sought to examine whether activity in the NAc→LH pathway is necessary for preventing relapse caused by PVT→NAc pathway inhibition. We injected retrograde AAV expressing Cre recombinase (rAAV2-retro-Cre) into the LH and Cre-dependent AAV expressing hM4D (AAV-DIO-hM4D) in the NAc to achieve selective expression of hM4D in the NAc^{LH} neurons. We also injected AAV8-hM4D into the PVT of the same mouse. Local infusion of CNO into the NAc of these mice inhibits both terminals of the PVT→NAc pathway and cell bodies of the retrogradely labeled NAc^{LH} neurons (Figure 5F). We found that simultaneous inhibition of both pathways diminished the effect of PVT→NAc pathway silencing on CPP retrieval (test 2) and the following test 3 (Figure 5G). Therefore, PVT→NAc-pathway-silencing-caused disinhibition of the NAc→LH pathway is required for preventing CPP retrieval. Together, these results reveal an essential role of the PVT→NAc→LH pathway in the maintenance of morphine-associated memories and substantiate the utility of the $iDISCO^+$ activity mapping method to identify novel behaviorally relevant pathways.

DISCUSSION

In this study, we examined roles of the PVT in contextual opiate-associated memories that drive relapse. Our results establish that the PVT is a critical node in the neural networks that orchestrate the formation and maintenance of opiate-associated memories through its connection with the CeA and NAc, respectively. A similar strategy has recently been found in hippocampal circuits, where distinct CA1 output pathways were used for the formation and retrieval of contextual fear memories (Roy et al., 2017). Interestingly, many neurons in the CA1 and PVT have collateralized axons that innervate downstream targets for both memory formation and retrieval. Thus, how distinct downstream targets engaged in different stages of memory are important questions for future study.

The PVT→CeA pathway has been shown to be important for fear memory formation (Do-Monte et al., 2015; Penzo et al., 2015). Here, we found that activation of this pathway has no behavioral effect in the real-time place preference assay, yet this pathway is required for associating drug reward with its environmental cues. Together with our recent observation that neurons in the PVT encode stimulus salience irrespective of valence (Zhu et al., 2018), we suggest that activity in the PVT→CeA pathway helps associate the salient effects of drug or foot shock to proximate cues. It has been reported that optogenetic activation of the CeA as a whole amplifies the incentive motivation and strongly biases choices toward the light-stimulation-paired reward (Robinson et al., 2014). It will be intriguing to see whether activation of the PVT→CeA pathway is sufficient to create bias toward a specific reward association, as drug addicts usually have narrow and biased choice toward drug rewards.

In contrast to the PVT→CeA pathway, inhibition of the PVT→NAc pathway has no effect on morphine reward learning. However, the maintenance of opiate-associated memories was entirely disrupted when this same pathway was inhibited during retrieval, which occurred 2 days after the last morphine exposure. Importantly, this transient inhibition completely prevented relapse to seeking the morphine-associated context even after a prolonged period of abstinence. Because the PVT→NAc pathway controls the expression of opioid withdrawal symptoms (Zhu et al., 2016), our data support a key role for the negative affective state during opioid abstinence in maintaining opiate-associated memories (Evans and Cahill, 2016). To further delineate the impact of PVT→NAc pathway inhibition on different memory processes, we inhibited this pathway at four time points: during CPP training, after last CPP training, during retrieval, and after retrieval test. Inhibition of the PVT→NAc pathway during retrieval, but not at other time points, prevented relapse, indicating that activity of this pathway is required for retrieval, but not consolidation and reconsolidation, of CPP memory and that inhibition of this pathway might effectively deepen extinction to prevent relapse (Gibson et al., 2018; Rescorla, 2006).

Furthermore, our results reveal a synaptic mechanism by which PVT→NAc inhibition affects downstream circuitry involved in storing opiate-associative memories. We showed

(D) Top panels: example of current injection induced AP traces of NAc^{LH} neurons from saline (black) and morphine (red) treated mice, with (blue background) and without 20 Hz photostimulation. Scale bars, 40 mV, 100 ms. Bottom panel: quantification of AP frequency. Photoactivation of PVT inputs increases AP firing in saline-treated mice (left, n = 8 cells) but decrease AP firing in morphine-treated mice (right, n = 10 cells). *p < 0.05; multiple t test with Bonferroni correction.
(E) Experimental timeline (upper panel), schematic (lower panel, left), and quantification of NAc→LH optogenetic activation during morphine CPP retrieval (lower panel, middle) and drug-primed relapse (lower panel, right). Light stimulation in ChR2-expressing mice (blue, tests 1–3, n = 9; tests 4 and 5, n = 6), but not EGFP-expressing mice (black, tests 1–3, n = 8; tests 4 and 5, n = 6) blocks the retrieval (test 2, test 3) and relapse (tests 4 and 5). Two-way ANOVAs (tests 1–3: main effect of group $F_{(1,15)} = 10.51$, p = 0.0036; main effect of test $F_{(2,30)} = 2.092$, p = 0.0665; interaction $F_{(2,30)} = 2.855$, p = 0.0346; tests 4 and 5: main effect of group $F_{(1,10)} = 10.48$, p = 0.0089; main effect of test $F_{(1,10)} = 0.0009$, p = 0.9764; interaction $F_{(1,20)} = 0.0449$, p = 0.8364). *p < 0.05; ***p < 0.001.
(F) Experimental design for inhibiting the PVT→NAc and NAc→LH pathways simultaneously. AAV8-hM4D was injected into the PVT, rAAV2-retro-cre was injected into the LH, and AAV9-DIO-hM4D was injected into the NAc. Cannulas were implanted into the NAc. Local infusion of CNO can inhibit both hM4D-expressing terminals of PVT inputs and the cell body of NAc^{LH} neurons.
(G) Histogram shows similar CPP scores between local infusion of saline (gray, n = 6) or CNO (red, n = 6) during test 2 and the following test 3.
Data are presented as mean ± SEM. See also Figures S4 and S5 and Table S2.

Please cite this article in press as: Keyes et al., Orchestrating Opiate-Associated Memories in Thalamic Circuits, Neuron (2020), https://doi.org/10.1016/j.neuron.2020.06.028

that repeated morphine converts the effect of PVT inputs onto NAc^{LH} neurons from excitation to inhibition. Therefore, inhibition of the PVT→NAc pathway in morphine-dependent animals would disinhibit NAc^{LH} neurons, and indeed, we demonstrated that transient activation of the NAc→LH pathway is sufficient to protect against relapse. Moreover, inhibition of the NAc→LH pathway completely abolished memory retrieval and relapse prevention caused by the inhibition of the PVT→NAc pathway, which supports model that disinhibition of the NAc→LH pathway underlies the beneficial effect of PVT→NAc pathway inhibition. Together, these results reveal a neural mechanism by which morphine alters the PVT→NAc→LH circuit to maintain the contextual association and drive morphine seeking. Because the NAc→LH pathway has also been shown to be important for seeking other rewards, such as food and alcohol (Gibson et al., 2018; O'Connor et al., 2015), it will be interesting to examine whether a similar synaptic mechanism occurs in these contexts. If so, the PVT→NAc→LH circuit could be a general target for treating addiction. Finally, our unbiased brain-wide activity mapping also identified many brain regions that previously had not been linked to opioid relapse. Studying these regions may lead to the identification of new circuitries or molecules that could treat opioid addiction.

STAR★METHODS

Detailed methods are provided in the online version of this paper and include the following:

- KEY RESOURCES TABLE
- RESOURCE AVAILABILITY
  - Lead Contact
  - Materials Availability
  - Data and Code Availability
- EXPERIMENTAL MODEL AND SUBJECT DETAILS
- METHOD DETAILS
  - Surgery
  - Behavioral assays
  - Morphine CPP with chemogenetic inhibition
  - Morphine CPP with optogenetic inhibition during retrieval test
  - Suboptimal morphine CPP
  - Hedonic eating assay
  - Real-time place preference assay
  - Morphine CPP with optogenetic activation during retrieval test
  - Morphine relapse test
  - iDISCO$^+$ Sample Processing (Renier et al., 2014, 2016)
  - ClearMap Analysis
  - Electrophysiological recording
  - Fiber photometry
- QUANTIFICATION AND STATISTICAL ANALYSIS

SUPPLEMENTAL INFORMATION

Supplemental Information can be found online at https://doi.org/10.1016/j.neuron.2020.06.028.

ACKNOWLEDGMENTS

We thank Dr. Robert C. Malenka, Dr. Liqun Luo, and other Chen lab members for helpful comments on the manuscript and the Luo lab for the use of the light-sheet microscope. We thank K.K. Zhou, F.L. Li, and G.Q. Hou for their help with parts of the CPP and electrophysiology experiments. This work was supported by grants from the Whitehall Foundation, the Firmenich Next Generation Fund, the Terman Fellowship, the Wu Tsai Neurosciences Institute's NeuroChoice Initiative, National Institutes of Health grants R01DA045664, R01MH116904, and R01HL150566 to X.K. G.N. is partially supported by a training grant from the National Institute on Drug Abuse (5T32DA035165-02). Y.J.Z. is supported by a NARSAD Young Investigator Grant by the Brain & Behavior Research Foundation (25282), a Shenzhen governmental grant (JCYJ20180507182420114), a Guangzhou Regenerative Medicine and Health-Guangdong Laboratory Research Grant (2018GZR110105006), the National Natural Science Foundation of China (81922024), the Guangdong Provincial Key Laboratory of Brain Connectome and Behavior (2017B030301017), and the Chinese Academy of Sciences International Partnership Program (172644KYSB20170004).

AUTHOR CONTRIBUTIONS

X.C. conceived the study. P.C.K., G.N., and X.C. designed the experiments and analyzed data. P.C.K. conducted behavioral experiments with help from and Y.Z. and V.J.W. P.C.K. and E.L.A conducted iDISCO$^+$ experiments in M.T.-L.'s laboratory. Z.C., Y.Z., and L.B. conducted slice recording. P.C.K., G.N., and X.C. wrote the manuscript with input from all authors.

DECLARATION OF INTERESTS

The authors declare no competing interests.

Received: June 3, 2019
Revised: May 28, 2020
Accepted: June 23, 2020
Published: July 16, 2020

REFERENCES

Alexander, G.M., Rogan, S.C., Abbas, A.I., Armbruster, B.N., Pei, Y., Allen, J.A., Nonneman, R.J., Hartmann, J., Moy, S.S., Nicolelis, M.A., et al. (2009). Remote control of neuronal activity in transgenic mice expressing evolved G protein-coupled receptors. Neuron *63*, 27–39.

Armbruster, B.N., Li, X., Pausch, M.H., Herlitze, S., and Roth, B.L. (2007). Evolving the lock to fit the key to create a family of G protein-coupled receptors potently activated by an inert ligand. Proc. Natl. Acad. Sci. USA *104*, 5163–5168.

Bossert, J.M., Marchant, N.J., Calu, D.J., and Shaham, Y. (2013). The reinstatement model of drug relapse: recent neurobiological findings, emerging research topics, and translational research. Psychopharmacology (Berl.) *229*, 453–476.

Boyden, E.S., Zhang, F., Bamberg, E., Nagel, G., and Deisseroth, K. (2005). Millisecond-timescale, genetically targeted optical control of neural activity. Nat. Neurosci. *8*, 1263–1268.

Chen, T.W., Wardill, T.J., Sun, Y., Pulver, S.R., Renninger, S.L., Baohan, A., Schreiter, E.R., Kerr, R.A., Orger, M.B., Jayaraman, V., et al. (2013). Ultrasensitive fluorescent proteins for imaging neuronal activity. Nature *499*, 295–300.

Chow, B.Y., Han, X., Dobry, A.S., Qian, X., Chuong, A.S., Li, M., Henninger, M.A., Belfort, G.M., Lin, Y., Monahan, P.E., and Boyden, E.S. (2010). High-performance genetically targetable optical neural silencing by light-driven proton pumps. Nature *463*, 98–102.

Cui, G., Jun, S.B., Jin, X., Pham, M.D., Vogel, S.S., Lovinger, D.M., and Costa, R.M. (2013). Concurrent activation of striatal direct and indirect pathways during action initiation. Nature *494*, 238–242.

Do-Monte, F.H., Quiñones-Laracuente, K., and Quirk, G.J. (2015). A temporal shift in the circuits mediating retrieval of fear memory. Nature *519*, 460–463.

Dobbs, L.K., Kaplan, A.R., Lemos, J.C., Matsui, A., Rubinstein, M., and Alvarez, V.A. (2016). Dopamine regulation of lateral inhibition between striatal neurons gates the stimulant actions of cocaine. Neuron *90*, 1100–1113.

Evans, C.J., and Cahill, C.M. (2016). Neurobiology of opioid dependence in creating addiction vulnerability. F1000Res. *5*, F1000.

Fadok, J.P., Markovic, M., Tovote, P., and Lüthi, A. (2018). New perspectives on central amygdala function. Curr. Opin. Neurobiol. *49*, 141–147.

Gibson, G.D., Prasad, A.A., Jean-Richard-Dit-Bressel, P., Yau, J.O.Y., Millan, E.Z., Liu, Y., Campbell, E.J., Lim, J., Marchant, N.J., Power, J.M., et al. (2018). Distinct accumbens shell output pathways promote versus prevent relapse to alcohol seeking. Neuron *98*, 512–520.e516.

Gunaydin, L.A., Grosenick, L., Finkelstein, J.C., Kauvar, I.V., Fenno, L.E., Adhikari, A., Lammel, S., Mirzabekov, J.J., Airan, R.D., Zalocusky, K.A., et al. (2014). Natural neural projection dynamics underlying social behavior. Cell *157*, 1535–1551.

Han, X., Chow, B.Y., Zhou, H., Klapoetke, N.C., Chuong, A., Rajimehr, R., Yang, A., Baratta, M.V., Winkle, J., Desimone, R., and Boyden, E.S. (2011). A high-light sensitivity optical neural silencer: development and application to optogenetic control of non-human primate cortex. Front. Syst. Neurosci. *5*, 18.

Kirouac, G.J. (2015). Placing the paraventricular nucleus of the thalamus within the brain circuits that control behavior. Neurosci. Biobehav. Rev. *56*, 315–329.

Koob, G.F., and Volkow, N.D. (2010). Neurocircuitry of addiction. Neuropsychopharmacology *35*, 217–238.

Li, S., and Kirouac, G.J. (2008). Projections from the paraventricular nucleus of the thalamus to the forebrain, with special emphasis on the extended amygdala. J. Comp. Neurol. *506*, 263–287.

Lüscher, C. (2016). The emergence of a circuit model for addiction. Annu. Rev. Neurosci. *39*, 257–276.

Millan, E.Z., Ong, Z., and McNally, G.P. (2017). Paraventricular thalamus: gateway to feeding, appetitive motivation, and drug addiction. Prog. Brain Res. *235*, 113–137.

Milton, A.L., and Everitt, B.J. (2012). The persistence of maladaptive memory: addiction, drug memories and anti-relapse treatments. Neurosci. Biobehav. Rev. *36*, 1119–1139.

Monfils, M.H., Cowansage, K.K., Klann, E., and LeDoux, J.E. (2009). Extinction-reconsolidation boundaries: key to persistent attenuation of fear memories. Science *324*, 951–955.

Nader, K., Schafe, G.E., and Le Doux, J.E. (2000). Fear memories require protein synthesis in the amygdala for reconsolidation after retrieval. Nature *406*, 722–726.

O'Connor, E.C., Kremer, Y., Lefort, S., Harada, M., Pascoli, V., Rohner, C., and Lüscher, C. (2015). Accumbal D1R neurons projecting to lateral hypothalamus authorize feeding. Neuron *88*, 553–564.

Penzo, M.A., Robert, V., Tucciarone, J., De Bundel, D., Wang, M., Van Aelst, L., Darvas, M., Parada, L.F., Palmiter, R.D., He, M., et al. (2015). The paraventricular thalamus controls a central amygdala fear circuit. Nature *519*, 455–459.

Renier, N., Wu, Z., Simon, D.J., Yang, J., Ariel, P., and Tessier-Lavigne, M. (2014). iDISCO: a simple, rapid method to immunolabel large tissue samples for volume imaging. Cell *159*, 896–910.

Renier, N., Adams, E.L., Kirst, C., Wu, Z., Azevedo, R., Kohl, J., Autry, A.E., Kadiri, L., Umadevi Venkataraju, K., Zhou, Y., et al. (2016). Mapping of brain activity by automated volume analysis of immediate early genes. Cell *165*, 1789–1802.

Rescorla, R.A. (2006). Deepened extinction from compound stimulus presentation. J. Exp. Psychol. Anim. Behav. Process. *32*, 135–144.

Robinson, M.J., Warlow, S.M., and Berridge, K.C. (2014). Optogenetic excitation of central amygdala amplifies and narrows incentive motivation to pursue one reward above another. J. Neurosci. *34*, 16567–16580.

Roy, D.S., Kitamura, T., Okuyama, T., Ogawa, S.K., Sun, C., Obata, Y., Yoshiki, A., and Tonegawa, S. (2017). Distinct neural circuits for the formation and retrieval of episodic memories. Cell *170*, 1000–1012.e1019.

Rudd, R.A., Seth, P., David, F., and Scholl, L. (2016). Increases in drug and opioid-involved overdose deaths—United States, 2010-2015. MMWR Morb. Mortal. Wkly. Rep. *65*, 1445–1452.

Shaham, Y., Shalev, U., Lu, L., de Wit, H., and Stewart, J. (2003). The reinstatement model of drug relapse: history, methodology and major findings. Psychopharmacology (Berl.) *168*, 3–20.

Stachniak, T.J., Ghosh, A., and Sternson, S.M. (2014). Chemogenetic synaptic silencing of neural circuits localizes a hypothalamus→midbrain pathway for feeding behavior. Neuron *82*, 797–808.

Tervo, D.G., Hwang, B.Y., Viswanathan, S., Gaj, T., Lavzin, M., Ritola, K.D., Lindo, S., Michael, S., Kuleshova, E., Ojala, D., et al. (2016). A designer AAV variant permits efficient retrograde access to projection neurons. Neuron *92*, 372–382.

Tzschentke, T.M. (2007). Measuring reward with the conditioned place preference (CPP) paradigm: update of the last decade. Addict. Biol. *12*, 227–462.

Venniro, M., Caprioli, D., and Shaham, Y. (2016). Animal models of drug relapse and craving: from drug priming-induced reinstatement to incubation of craving after voluntary abstinence. Prog. Brain Res. *224*, 25–52.

White, N.M. (1996). Addictive drugs as reinforcers: multiple partial actions on memory systems. Addiction *91*, 921–949, discussion 951–965.

Wise, R.A., and Koob, G.F. (2014). The development and maintenance of drug addiction. Neuropsychopharmacology *39*, 254–262.

Xue, Y.X., Luo, Y.X., Wu, P., Shi, H.S., Xue, L.F., Chen, C., Zhu, W.L., Ding, Z.B., Bao, Y.P., Shi, J., et al. (2012). A memory retrieval-extinction procedure to prevent drug craving and relapse. Science *336*, 241–245.

Zhu, Y., Wienecke, C.F., Nachtrab, G., and Chen, X. (2016). A thalamic input to the nucleus accumbens mediates opiate dependence. Nature *530*, 219–222.

Zhu, Y., Nachtrab, G., Keyes, P.C., Allen, W.E., Luo, L., and Chen, X. (2018). Dynamic salience processing in paraventricular thalamus gates associative learning. Science *362*, 423–429.

Please cite this article in press as: Keyes et al., Orchestrating Opiate-Associated Memories in Thalamic Circuits, Neuron (2020), https://doi.org/10.1016/j.neuron.2020.06.028

STAR★METHODS

KEY RESOURCES TABLE

REAGENT or RESOURCE	SOURCE	IDENTIFIER
Antibodies		
Rabbit polyclonal anti-c-Fos	Santa Cruz Biotechnology	SC-52G; RRID:AB_2629503
Donkey anti-rabbit 647	Invitrogen	A-31573; RRID:AB_2536183
Bacterial and Virus Strains		
AAV1.hSyn.eGFP.WPRE.bGH	a gift from Bryan Roth	Addgene: 50465-AAV1
AAV1.hSynp.hChR2(H134R)-eYFP.WPRE.hGH	a gift from Karl Deisseroth	Addgene: 26973-AAV1
AAV1.CAG.ArchT.GFP.WPRE.SV40	Han et al., 2011	Addgene: 29777-AAV1
AAV8.hSynp.hM4D-mCherry	This manuscript	N/A
rAAV2-retro-CAG.nls-mRuby3	This manuscript	N/A
AAV9-hEF1a-DIO-hM4D-mCherry-WPRE-pA	Taitool Bioscience	N/A
rAAV2-retro-CMV-bGI-Cre-EGFP-pA	Taitool Bioscience	N/A
AAV9.hSyn.GCaMP6m	BrainVTA Co.,Ltd.	N/A
Chemicals, Peptides, and Recombinant Proteins		
Morphine sulfate	West-Ward Pharmaceuticals	0641-6127-25
Clozapine N-oxide	Enzo Life Sciences	BML-NS105-0025
Cesium methanesulfonate	Sigma-Aldrich	C1426-5G
Strontium chloride	Sigma-Aldrich	439665-5G
QX 314 bromide	Tocris	1014
Experimental Models: Organisms/Strains		
Mouse C57BL/6J	Jackson Labs	000664
Mouse C57BL/6J	Beijing Vital River Laboratory Animal Technology Co., Ltd	N/A
Software and Algorithms		
MATLAB R2014a	The MathWorks, Inc.	N/A
pCLAMP10.6	Molecular Devices	N/A

RESOURCE AVAILABILITY

Lead Contact

Further information and requests for resources and reagents should be directed to and will be fulfilled by the Lead Contact, Xiaoke Chen (xkchen@stanford.edu).

Materials Availability

Plasmids generated in this study for virus production are available upon reasonable requests.

Data and Code Availability

Datasets are available upon reasonable requests. iDISCO c-Fos mapping data were analyzed using open source ClearMap software. The latest version of ClearMap can be downloaded from https://www.idisco.info/.

EXPERIMENTAL MODEL AND SUBJECT DETAILS

Male adult (5-12 weeks) C57BL/6 mice were used for all experiments. All procedures were in accordance with the US National Institute of Health guidelines for care and use of laboratory animals and were approved by Stanford University's Administrative Panel on Laboratory Animal Care.

Please cite this article in press as: Keyes et al., Orchestrating Opiate-Associated Memories in Thalamic Circuits, Neuron (2020), https://doi.org/10.1016/j.neuron.2020.06.028

CellPress

METHOD DETAILS

Surgery

Stereotaxic surgeries were performed on 5- to 7-week old mice under ketamine and xylazine (100 mg/Kg and 10 mg/Kg, i.p.) anesthesia using a stereotaxic instrument (BenchMARK Digital, Lecia). Virus was injected into the PVT (200 nl AAV, bregma −1.4 mm; lateral 0.1 mm; ventral 3.0 mm, with a 4° angle toward the midline), medial shell of the NAc (200 nl AAV, bregma 1.1 mm; lateral 0.8 mm; ventral 4.6 mm), or LH (200 nL AAV, bregma 1.58 mm; latera 1.6 mm; ventral 5.5 mm) with a pulled glass capillary at a slow rate (100 nL min^{-1}) using a pressure microinjector (Micro 4 system, World Precision Instruments). The injection capillary was removed 5 min after the end of the injection. For mice used for behavioral experiments, an infusion or fiber-optic cannula (Plastics One) was placed at least 500 μM above the target brain region (NAc, LH, or CeA: bregma −1.25 mm; latera 2.9 mm; ventral 5.25 mm) and cemented to the skull using dental cement (Lang Dental Manufacturing). After surgery, a dummy cannula was inserted and a cap was screwed on to keep the guide cannula from becoming occluded. Mice were allowed at least 2 weeks to recover and to express the virus before behavioral training commenced. AAVs used in this study were produces the University of Pennsylvania vector core/addgene: AAV1.hSyn.eGFP.WPRE.bGH, 1.8 × 10^{13} genomic copies ml^{-1}; AAV1.hSynp.hChR2(H134R)-eYFP.WPRE.hGH, 8.0 × 10^{12} genomic copies ml^{-1}; AAV5.CAG.ArchT.GFP.WPRE.SV40, 1.8 × 10^{13} genomic copies ml^{-1}; or in-house: AAV8.hSynp.hM4D-mCherry, 8.3 × 10^{12} genomic copies ml^{-1}; rAAV2-retro-CAG.nls-mRuby3, 2.3 × 10^{13} genomic copies ml^{-1}.

Behavioral assays

All mice used in behavioral assays were allowed to recover from surgery of AAV injection and cannula implantation for at least 2 weeks. Place preference training was performed in a custom-made two-compartment conditioned place preference (CPP) apparatus (30 cm × 25 cm × 20 cm). All locomotor behaviors, including real-time place preference and conditioned place preference, were recorded for 15–20 min at 30 frames per second with a camera controlled by custom tracking software running on MATLAB (MathWorks). CPP scores were calculated by subtracting the time spent in the morphine-paired side of the chamber during baseline from the time spent in the same side of the chamber during the test.

Morphine CPP with chemogenetic inhibition

Mice infected with AAV-hM4D–mCherry or AAV-tdTomato in the PVT were allowed to freely explore both sides of a custom-made CPP training apparatus for 15 min to assess their baseline place preference. Then, for chemogenetic inhibition during CPP formation, these mice were injected with saline (i.p.) and confined to their preferred side of the chamber for 45 min then returned to their home cage. At least four hours later, the same mice received a local infusion of CNO (3 μM, 200 nl) into the NAc or CeA 20 min before an i.p. injection of 15 mg/Kg morphine and were confined to their non-preferred side of the chamber for 45 minutes. They then were returned to their home cage. The same training with saline and CNO infusion will performed for four consecutive days. Twenty-four hours after the final training session, mice were re-exposed to the CPP chamber and allowed to explore both sides of the chamber for 15 min. For chemogenetic inhibition during retrieval test, separate groups of AAV-hM4D–mCherry or AAV-tdTomato injected mice will went through 4 days of above mentioned CPP training without CNO infusion. Twenty-four hours after the final training session, mice were re-exposed to the CPP chamber and allowed to explore both sides of the chamber for 15 minutes (test1). Mice that did not show a strong preference for the morphine-paired chamber (< 90 s) were excluded from further behavioral assays. Another twenty-four hours later, we infuse saline or CNO into the mice 20 min before reintroduced the mice to the CPP chamber for 15 minutes of free exploration (test 2). Finally, another twenty-four hours later, mice were reintroduced into the CPP chamber and allowed to freely explore for 15 minutes (test 3). For chemogenetic inhibition after retrieval test 2 (Figure 3G), the mice underwent an identical CPP protocol as described with the single difference that CNO or saline infusion occurred immediate after the test 2 time point.

Morphine CPP with optogenetic inhibition during retrieval test

Mice infected with AAV-ArchT-YFP or AAV-eGFP injected in the PVT were allowed to freely explore both sides of a custom-made CPP training apparatus for 15 min to assess their baseline place preference. Then, for four consecutive days, these mice were injected with saline (i.p.) and confined to their preferred side of the chamber for 45 min then returned to their home cage. At least four hours later, the same mice received an i.p. injection of 15 mg/Kg morphine and were confined to their non-preferred side of the chamber for 45 minutes. They then were returned to their home cage. Twenty-four hours after the final training session, mice were re-exposed to the CPP chamber and allowed to explore both sides of the chamber for 15 min (test1). Mice that did not show a strong preference for the morphine-paired chamber (< 90 s) were excluded from further behavioral assays. Another twenty-four hours later, we inserted optical fibers into the NAc or CeA for optogenetic inhibition with green lasers (532 nm, 5 mW mm^{-2}) and reintroduced the mice to the CPP chamber for 15 minutes of free exploration (test 2). Finally, another twenty-four hours later, mice were reintroduced into the CPP chamber and allowed to freely explore for 15 minutes (test 3). For inhibition in the novel context in Figures 2D and 3F, the mice underwent an identical CPP protocol as described with the single difference that inhibition occurred in a novel cage at the test 2 time point.

Please cite this article in press as: Keyes et al., Orchestrating Opiate-Associated Memories in Thalamic Circuits, Neuron (2020), https://doi.org/10.1016/j.neuron.2020.06.028

Suboptimal morphine CPP

Mice infected with AAV-ChR2-YFP or AAV-eGFP in the PVT underwent a similar behavioral paradigm as described above with small variations. First, mice were injected with a lower dose of morphine (5 mg/Kg). Second, training sessions lasted only 15 minutes. Finally, there were only three days of training. Additionally, optical fibers were inserted into the CeA and blue light (473 nm, 20 ms pulses, 4 mW mm^{-2}) was delivered during the morphine training sessions.

Hedonic eating assay

Mice infected with AAV-hM4D–mCherry in the PVT were exposed to mini M&Ms in their home cage for three consecutive days along with their normal food. On the fourth day, these well-fed mice were infused with PBS into the CeA and placed into a novel environment with three mini M&Ms for 40 min. Twenty-four hours later, the same mice were infused with CNO (3 μM, 200 nl) into the CeA and again placed into the novel environment with three mini M&Ms for 40 min. The amount of chocolate consumed was calculated by weighing the mini M&Ms before and after the 40 min period.

Real-time place preference assay

After connecting with optical fibers, mice infected with AAV-ChR2-YFP or AAV-eGFP in the PVT were placed in the CPP training apparatus to freely explore for 15 minutes. When the mouse crossed to the stimulated side of the chamber, it triggered 20 Hz laser stimulation (473 nm, 20 ms pulses, 7 mW mm^{-2} at the CeA) until the mouse crossed back to the non-stimulated side. Preference score was calculated by measuring the percent of the time that the animal spent on the light paired side of the chamber.

Morphine CPP with optogenetic activation during retrieval test

Mice infected with AAV-ChR2-YFP or AAV-eGFP in the NAc followed an identical experimental protocol as described above except during test 2, optical fibers were connected for delivery of blue lasers (473 nm, 20 ms pulses, 4 mW mm^{-2}) aimed at the LH.

Morphine relapse test

Mice that were used in activation or inhibition during morphine CPP test were injected with a priming dose of morphine (10 mg/Kg, i.p.) 4 days after the final training session (test 4) and re-exposed to the CPP chamber for 15 min of free exploration. 10 days later (test 5), the same mice were injected with a priming dose of morphine again and re-exposed to the CPP chamber to freely explore for 15 minutes.

iDISCO$^+$ Sample Processing (Renier et al., 2014, 2016)

Same mice that underwent optogenetic inhibition during test 2 and morphine relapse test (Figures 3C and 3D) were euthanized with a rising gradient of CO_2 and their brains were fixed by intracardial perfusion of 4% paraformaldehyde (PFA) in PBS 60 min after the final behavioral assay. Brains were then post-fixed in PFA at 4°C overnight in 5ml Eppendorf tubes. The following day brains were washed in PBS with 0.02% NaN_3 three times for 30 minutes then left in PBS with NaN_3 for two days at 4°C in new 5 ml tubes. Brains were then dehydrated using a freshly prepared dilution series of methanol (MeOH) in PBS with NaN_3. Brains were washed in 20%, 40%, 60%, 80%, and 100% MeOH for 30 min to 3 hours followed by a final 30 min 100% MeOH wash in a new tube. Brains were then put on ice and transferred to a 5% H_2O_2 bleach solution, prepared by diluting 30% H_2O_2 in MeOH on ice, and stored at 4°C overnight. The following day brains were allowed to warm to room temperature before being rehydrated with another freshly mixed MeOH/PBS dilution series. Here, brains were washed in 80%, 60%, 40%, 20% MeOH in PBS with NaN_3 for 30 min to 3 hours. Brains were transferred to new tubes before a final 1 hour wash in PBS with NaN_3. Brains were then transferred to a new tube filled with permeabilization solution (400 ml PBS/0.2% Triton/11.5g Glycine/100 mL DMSO/1 μL NaN_3) for two days kept rotating at 37°C. Then brains were washed in PTwH (100 ml 10x PBS/2ml Tween-20/1ml of 10mg/μl Heparin/1 μL NaN_3/ddH_2O to 1L) two times for 5 min then transferred to a new tube filled with blocking solution (PBS with NaN_3/0.2% Triton/10% DMSO/6% donkey serum) and left rotating for 2 days at 37°C. Brains were then transferred to primary antibody solution (PTwH/5%DMSO/3% donkey serum, 1:500 Santa Cruz rabbit anti-c-Fos) and left rotating for 7 days at 37°C. Brains were then removed from primary antibody and washed three times in PTwH for 5 min, then every few hours for the rest of the day. The following day brains were placed in secondary antibody solution (PTwH/3% donkey serum, 1:500 Alexa Fluor donkey anti-rabbit 647) and kept rotating at 37°C for 7 days. Samples were exposed to minimal light from this step onward. After 7 days samples were washed in PTwH three times for 5 min then every few hours for the rest of the day and the following day. The next day samples were again dehydrated in a MeOH/ddH_2O series of 20%, 40%, 60%, 80%, and 100% MeOH for 30 min to 3 hours. Brains were transferred to a new tube for a final 1 hr 100% MeOH wash. Brains were then transferred to a solution comprised of 66% dichloromethane and 33% MeOH and left washing overnight at room temperature. The following day, the brains were washed twice in 100% DCM for 15 minutes and then transferred to a new tube containing dibenzyl ether and left to clear for three days before imaging. Brains were imaged in coronal and sagittal orientations using a light-sheet microscope (Ultramicroscope II, LaVision Biotec) with a CMOS camera (Andor Neo) and a 2x/0.5 objective lens (MVLAPO 2x). Samples were imaged in the 640 nm channel at 0.8x using a 3 μm step size.

ClearMap Analysis

iDISCO c-Fos mapping datasets were analyzed with open source ClearMap software using methods similar to those described previously (Renier et al., 2016). Fos$^+$ neurons were detected using the 3D cell detection modal in Clearmap. To tune the algorithm and

Please cite this article in press as: Keyes et al., Orchestrating Opiate-Associated Memories in Thalamic Circuits, Neuron (2020), https://doi.org/10.1016/j.neuron.2020.06.028

filters, we manually annotated all the cells in a substack of our datasets, then iterated the parameters of the filter to achieve maximal overlap between the manual and automatic annotations. 3D datasets were registered to the Allen Brain Atlas 25 μm map using the 488 nm autofluorescence image stake. The number of Fos^+ neurons per brain region was first normalized by the volume of the same area in the Allen Brain Atlas, then compared between different groups using the independent Student's t test.

Electrophysiological recording

Procedures for preparing acute brain slices and performing whole-cell recordings with optogenetic stimulations were similar to those described previously (Zhu et al., 2016). Coronal 250–300 μM slices containing the NAc were prepared using a vibratome (VT-1000S, Leica) in an ice-cold choline-based solution containing (in mM) 110 choline chloride, 2.5 KCl, 0.5 $CaCl_2$, 7 $MgCl_2$, 1.3 NaH_2PO_4, 1.3 Na-ascorbate, 0.6 Na-pyruvate, 25 glucose and 25 $NaHCO_3$, saturated with 95% O_2 and 5% CO_2. Slices were incubated in 32°C oxygenated artificial cerebrospinal fluid (in mM: 125 NaCl, 2.5 KCl, 2 $CaCl_2$, 1.3 $MgCl_2$, 1.3 NaH_2PO_4, 1.3 Na-ascorbate, 0.6 Na-pyruvate, 25 glucose and 25 $NaHCO_3$) for at least 1 h before recording. Slices were transferred to a recording chamber and superfused with 2 ml min^{-1} artificial cerebrospinal fluid. Patch pipettes (2–5 MΩ) pulled from borosilicate glass (PG10150-4, World Precision Instruments) were filled with a Cs-based low Cl^- internal solution containing (in mM) 135 $CsMeSO_3$, 10 HEPES, 1 EGTA, 3.3 QX-314, 4 Mg-ATP, 0.3 Na-GTP, 8 Na_2-phosphocreatine, 290 mOsm kg^{-1}, adjusted to pH 7.3 with CsOH. Whole-cell voltage-clamp recording was performed at room temperature (22–25 °C) with a Multiclamp 700B amplifier and a Digidata 1440A (Molecular Devices). Data were sampled at 10 kHz and analyzed with pClamp10 (Molecular Devices) or MATLAB (MathWorks). The NAc^{LH} neuron were labeled by injection of AAV2-retro-CAG.nls-mRuby3 into the LH and visualized using an upright fluorescent microscope (Olympus BX51WI). A blue light-emitting diode (470 nm, Thorlabs) controlled by digital commands from the Digidata 1440A was coupled to the microscope with a dual lamp house adaptor (5-UL180, Olympus) to deliver photostimulation. To record action potential firing, a step current (60–150 pA) was injected at current clamp configuration. To record light-evoked EPSCs and IPSCs, 3–5 ms, 0.5–2 mW blue light was delivered through the objective to illuminate the entire field of view. To assess the efficiency of chemogenetic inhibition of synaptic transmission (Figure S5A), we first co-injected AAV-hM4D and AAV-ChR2 into the PVT, then prepared CeA slices containing the ChR2 and hM4D co-expressed terminals from the PVT. Light-evoked EPSCs were recorded from CeA neurons before and after perfusion with CNO (3 μM). Membrane potential was held at −70 mV to record EPSCs, at 0 mV to record GABAA receptor-mediated IPSCs. EPSC/IPSC ratios were calculated by dividing the amplitude of the EPSCs by the amplitude of the IPSCs.

To determine quantal synaptic response size at PVT→NAc synapses, calcium was replaced in the external solution with strontium, which induced asynchronous vesical release. Light (455 nm) was delivered for a duration of 2-5 ms to activate ChR2 at PVT→NAc axonal terminal. Recording was targeted to NAc^{LH} neuron which was labeled by retrograde tracer CTB. Individual sweeps were separated by 20 s. The mEPSC was recorded at holding potentials of −70 mV and mIPSC was recorded at holding potentials of 0 mV. To identify individual mEPSC/mIPSC events, a custom mEPSC/mIPSC template, 18 ms in duration, was created by averaging 250 manually selected events across multiple cells. To detect fluctuations in postsynaptic current, this template was then applied to the region of individual current traces, which was typically 60-500 ms post light stimulation. Event analysis was performed using pClamp10 software and a matching threshold of 2.8 was applied in order to minimize false positives.

Fiber photometry

Fiber photometry experiments were performed at least 3 weeks after AAV-GCaMP6m injection. The implanted fiber was connected to Fiber Optic Meter (ThinkerTech, Nanjing, China) through an optical fiber patch cord (200 μm, 0.37 NA, Inper, Hangzhou, China). To record fluorescence signals, a beam from a 480 LED was reflected with a dichroic mirror, focused with a lens coupled to an CMOS detector (Thorlabs, Inc. DCC3240M). The LED power at the tip of the patch cord was less than 50 μW. A Labview program was used to control the CMOS camera which recorded calcium signals at 50 Hz.

To record PVT→NAc or PVT→CeA pathway calcium activity, mice infected with GCaMP6m was trained with the identical CPP protocol as described above. To minimize photobleaching and potential fiber damage, pathway calcium activity was collected for 20 min during CPP acquisition and retrieval session. Analysis of the signal was done with custom-written MATLAB software. The fluorescence change (ΔF/F) was calculated as $(F-F_0)/F_0$, where F_0 is the baseline fluorescence signal. Events was identified as the peak that exceeded the mean by one standard deviation. The area under the curve (AUC) was calculated as mean ΔF/F of the event.

QUANTIFICATION AND STATISTICAL ANALYSIS

No statistics were used to predetermine sample size. However, our sample sizes were similar to those reported in previous publications. Statistical methods are indicated when used. All analyses were performed using Prism (GraphPad software) and presented in Table S2. No method of randomization was used in any of the experiments. For ANOVA analyses, the variances were similar as determined by Brown–Forsythe test. Experimenters were not blind to group allocation in behavioral experiments, but CPP score and locomotion were measured automatically by custom tracking software running on MATLAB (MathWorks). All animals that finished the entire behavioral training and testing were included in analysis. Data are presented as mean ± SEM.